ARTICLES

Journal of Semiconductors
(2020) 41, 052202
doi: 10.1088/1674-4926/41/5/052202

I/P interface modification for stable and efficient perovskite solar cells

Jie Zhang[1, 2, 3, 4], Shixin Hou[1, 2, 3, 4], Renjie Li[1, 2, 3, 4], Bingbing Chen[1, 2, 3, 4], Fuhua Hou[1, 2, 3, 4], Xinghua Cui[1, 2, 3, 4], Jingjing Liu[1, 2, 3, 4], Qi Wang[1, 2, 3, 4], Pengyang Wang[1, 2, 3, 4, †], Dekun Zhang[1, 2, 3, 4], Ying Zhao[1, 2, 3, 4], and Xiaodan Zhang[1, 2, 3, 4, †]

[1]Institute of Photoelectronic Thin Film Devices and Technology of Nankai University, Tianjin 300350, China
[2]Key Laboratory of Photoelectronic Thin Film Devices and Technology of Tianjin, Tianjin 300350, China
[3]Collaborative Innovation Center of Chemical Science and Engineering (Tianjin), Tianjin 300072, China
[4]Renewable Energy Conversion and Storage Center of Nankai University, Tianjin 300072, China

Abstract: Interface engineering has played an increasingly essential role in the development of perovskite solar cells (PSCs). Herein, we adopted an effective and simple one-step interface passivation method on a FA-based perovskite to fabricate efficient and stable planar PSCs. The surface defects are reduced by the perovskite interface passivation layer incorporated between the hole transport and perovskite absorber layers, and then non-radiative recombination is suppressed while interfacial carrier extraction is enhanced. The passivated planar PSCs demonstrates 20.83% power conversion efficiency (PCE), which is caused by the simultaneous enhancement of the fill factor and open-circuit voltage. In addition, the device also shows great ambient and thermal stability. It retains 94% of its original PCE after 1000 h under ambient air without encapsulation as well as 90% of its initial efficiency after 400 h under continuous heating at 65 °C with encapsulation. This research provides a strategy for the development of efficient and stable PSCs.

Key words: planar perovskite solar cell; interfacial engineering; one-step solution; stability

Citation: J Zhang, S X Hou, R J Li, B B Chen, F H Hou, X H Cui, J J Liu, Q Wang, P Y Wang, D K Zhang, Y Zhao, and X D Zhang, I/P interface modification for stable and efficient perovskite solar cells[J]. *J. Semicond.*, 2020, 41(5), 052202. http://doi.org/10.1088/1674-4926/41/5/052202

1. Introduction

Organic–inorganic halide perovskite solar cells (PSCs) have been rapid developed in the past decade due to their unique properties, such as high carrier mobility, low-cost fabrication, adjustable band-gap, simple solution-based processes, and long carrier diffusion length, etc.[1–6]. The power conversion efficiency (PCE) of PSCs is rapidly improved from 3.8% to a certified 25.2%, and they are becoming a very appealing candidate for new generation photovoltaic materials[7–10]. FA-based absorbers are the most widely used materials in PSCs with enhanced thermal stability and less likely moisture-induced decomposition[11–13]. Crystal defects are harmful to devices' stability and performance due to the inducing of charge recombination and moisture permeation[14–16]. Most crystal defects are located at the grain boundaries and interface. For actually commercial deployment, high performance and stability are equally important. Toward this end, many kinds of methods have been taken into consideration[17–23]. Among them, surface modification methods have been adopted.

Interface passivation is increasingly essential for enhancing the performance of PSCs. For example, You *et al.* reported that excess PbI_2 on the surface or grain boundaries of perovskite films can suppress charge recombination[24]. Saliba *et al.* used polymeric interlayer between the perovskite and hole transport interface, which is helpful to passivate the perovskite and then reduce recombination. A PCE of 20.35% was obtained with the quite significant improvement in stability. The devices maintain about 90% of its original PCE for 1000 h under continuous illumination[25]. Han *et al.* reported the passivation of a chlorinated graphene oxide (Cl-GO) layer on perovskite films for reducing surface defects. The cell with the heterostructure maintained 90% PCE value at the maximum power point after 1000 h[26]. Recently, You *et al.* reported a method of perovskite films surface defect passivation by using an organic halide salt (phenethylammonium iodide) and a certificated PCE of 23.32% was achieved [9].

In this work, in order to reduce the interface iodide deficiency for FA-based PSCs, we adopted an interface passivation method by using MABr reacted with excess PbI_2 to form a perovskite passivation layer between the hole transport layer (HTL) and perovskite absorber interface. The result demonstrates a decrease in surface defects and non-radiative recombination, and an increase in carrier extraction. So that, we obtain an enhanced PCE of 20.83%, which is superior to the control device with a PCE of 18.39%. In addition, the device indicates outstanding stability of humidity and temperature.

2. Experimental section

2.1. Materials

Isopropyl alcohol (IPA), N,N-dimethylformamide (DMF)

Correspondence to: P Y Wang, pywang@nankai.edu.cn; X D Zhang, xdzhang@nankai.edu.cn
Received 24 FEBRUARY 2020; Revised 27 MARCH 2020.

Fig. 1. (Color online) Schematic diagram of the formation of passivation layer.

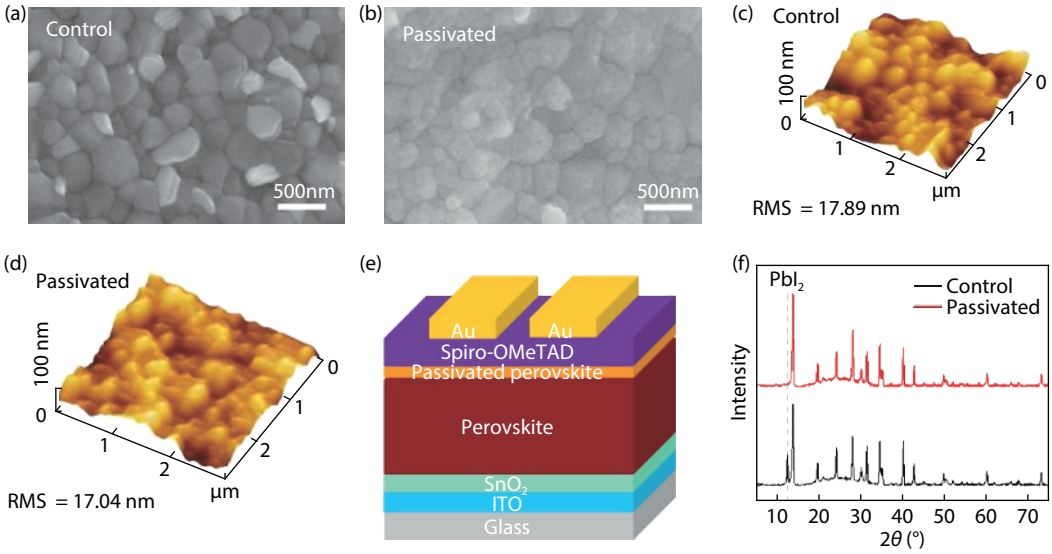

Fig. 2. (Color online) SEM and AFM images of (a, c) control and (b, d) passivated perovskite films on ITO/SnO_2 substrates. (e) Device structure of the passivated perovskite solar cells. (f) XRD patterns of passivated and control perovskite films.

and dimethylsulfoxide (DMSO) were obtained from Sigma Aldrich. SnO_2 precursor was purchased from Alfa Aesar. Other materials were obtained from Xi'an Polymer Light Technology Corp.

2.2. Film and device fabrication

First, the ITO glass substrates were immersed in industrial cleaning agents, acetone and isopropyl alcohol, for 40 min each for ultrasonic cleaning. Then they were put on the ultraviolet ozone machine platform and removed after 20 min of ozone treatment. The prepared tin dioxide solution (15% strength tin dioxide solution : ammonia = 1 : 3) was dropped on the ITO, which was spin-coated at a speed of 4000 rpm for 30 s, and then placed on a heating plate at 150 °C for 30 min. Ozone treatment was used for another 20 min. Dropped the configured FAMACs perovskite precursor solution containing FAI (1.1 M), PbI_2 (1.2 M), MABr (0.05 M), CsI (0.10 M), MACl (0.05 M) in mixture DMF : DMSO = 2 : 3 (v/v) on the tin dioxide layer, spin-coated at 1000 rpm for 10 s, then at 5000 rpm for 50 s during which in the last 20 s 100 μL of anti-solvent chlorobenzene was added. Put it directly on a 130 °C heating plate for 30 min. For the surface passivation treatment, cooled down the films to room temperature and dropped 60 μL of 2 mg/mL isopropyl alcohol solution containing MABr on the surface of the perovskite layer, and spin-coated it at a speed of 4000 rpm for 30 s, then placed it on a 90 °C heating plate for 5 min. Next, dropped 35 μL Spiro-OMeTAD on the surface of the passivation layer or perovskite layer, and then spin-coated at a speed of 4000 rpm for 30 s. At last, a layer of 80-nm gold top electrode was deposited by thermal evaporation.

2.3. Film and device characterization

The XRD patterns were obtained by Rigaku MiniFlex 600 using Kα radiation (λ = 1.5406 Å) to measure the crystal structure. In order to obtain the surface structure of the perovskite film, the SEM image was tested by FEI NanoSEM650. For getting the information of carrier lifetime, PL and TRPL tests were performed by fluorescence spectrophotometer (Edinburgh FS5). Current density–voltage (J–V) characteristics were obtained at the room temperature under AM 1.5G illumination by Keithley 2400 through a mask with an area of 0.089 cm^2. The dark density–voltage (J–V) characteristics were obtained under dark condition by Keithley 2400. The surface morphology of perovskite film was obtained by Nano-Navi-SPA400. The EQE spectra in ambient air were obtained by QEX10 instrument at room temperature.

3. Results and discussion

The formation process of perovskite passivation film is shown in Fig. 1. Proper amount of PbI_2 in grain boundaries could passivate the defects and deliver higher efficiency[24, 27]. While the excessive PbI_2 without light response, used for reacting by MABr to form passivation layer, the layer could passivate the defects and also being with enhanced light response.

The scanning electron microscopy (SEM) images of perovskite films with and without modification are shown in Figs. 2(a) and 2(b), respectively. It can be deduced that the surface of perovskite film with modification is flatter. From

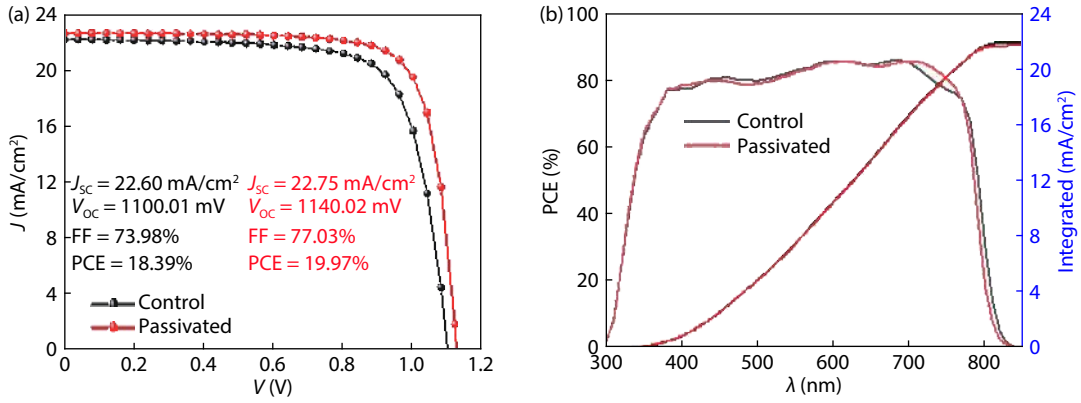

Fig. 3. (Color online) (a) *J*–*V* curves of the control and passivated perovskite solar cells. (b) External quantum efficiency (EQE) spectra for the passivated and control devices.

Table 1. Summary of the device performance with different concentrations of MABr treatment.

MABr concentration	J_{SC} (mA/cm^2)	V_{OC} (V)	FF (%)	Eff (%)
Control	22.60	1.10	73.98	18.39
1 mg/mL	22.61	1.10	77.01	19.15
2 mg/mL	22.75	1.14	77.03	19.97
3 mg/mL	22.53	1.13	76.47	19.46
4 mg/mL	21.90	1.10	74.08	17.84
5 mg/mL	21.98	1.14	70.02	17.54

Table 2. Summary of fitted results of TRPL of the passivated and control devices.

Sample	τ_1 (ns)	τ_2 (ns)	τ_1 (%)	τ_2 (%)	A_1	A_2
Control	13	182	22.27	77.73	620.89	123.49
Passivation	10	190	21.30	78.70	602.58	124.06

the atom force microscopy (AFM) measurement shown in Figs. 2(c) and 2(d), it can be regarded that the passivation layer results in smoother perovskite films. Root mean square (RMS) of the passivated and control films are 17.04 and 17.89 nm, respectively. Fig. 2(e) shows the device structure diagram of the passivated perovskite solar cells. The results of X-ray diffraction (XRD) are shown in Fig. 2(f). The diffraction peak of PbI_2 (12.6°) decreases sharply after spin-coating of the MABr, which indicats that a new perovskite is formed due to the reaction of excessive PbI_2 with MABr[24, 28]. Too much PbI_2 is detrimental to the hysteresis and stability of the device, which can also be reconfirmed in this work. Table 1 is the result of one batch of experiments, the best PCE is the device with concentration of 2 mg/mL MABr.

Fig. 3(a) shows the *I*–*V* relationship of the devices with and without I/P interface passivation. The efficiency increased from 18.39% to 19.97%. Current density did not change greatly, but the V_{oc} and the FF increased from 1.10 to 1.14 eV and from 73.98% to 77.03%, respectively. Fig. 3(b) shows the external quantum efficiency (EQE) spectra of the passivated and original devices. It can be found that the integrated current densities of control and passivated perovskite solar cell are 22.03 and 21.80 mA/cm^2, respectively, which shows the same trend with the *J*–*V* results.

Ultraviolet photoelectron spectroscopy (UPS) measurements of glass/ITO/perovskite and glass/ITO/perovskite/passivation substrates were used to further study the energy band structure[29, 30]. The data of the control and the passivated perovskite films are shown in Fig. 4(a). Helium Ⅰ ($h\nu$ = 21.22 eV) spectra of secondary electron cutoff band of the control and passivated perovskite films are 17.86 and 18.25 eV, respectively (Fig. 4(b)). The work functions (W_S) of the control and passivated perovskite films are 3.36 and 2.97 eV, respectively. The valence bands related to the Fermi level are 2.40 and 2.67 eV, respectively (Fig. 4(c)). By the calculation formula $E_V = W_S$ + VBM, we can get the calculated valence bands of the control and passivated films are 5.76 and 5.64 eV, respectively[31, 32]. After passivation, the valence band shifted by 0.12 eV relative to the control sample. Based on these measurements, we plotted the energy levels of these two thin films, which are shown in Fig. 4(d). The energy level for other films are obtained from previous published references[33]. It can be clearly seen that the passivated film has a better energy level matching with the lowest unoccupied molecular orbit (LUMO) level of Spiro than that of the control film, which can improve the carrier extraction capability. Fig. 4(e) shows the steady-state photoluminescence (PL) with the device structures of ITO/perovskite/passivation layer/spiro and ITO/perovskite/ spiro, respectively. As is well known, the lower PL intensity means better charge separation from the light absorbing layer to the carrier transport layer. By introducing passivation layer on the PVK surface, the PL intensity can be significantly reduced, which indicates that surface passivation improves the hole extraction[34, 35]. This can also be confirmed by time-resolved photoluminescence (TRPL) in Fig. 4(f). The TRPL decay curves of ITO/perovskite/passivation layer/spiro and ITO/perovskite/spiro were fitted with the following biexponential rate law[36].

$$Y = A_1\exp\left(-t/\tau_1\right) + A_2\exp\left(-t/\tau_2\right) + y_0.$$

Here, τ_1 and τ_2 are the fast and slow recombination lifetimes, and A_1 and A_2 are the relative amplitudes. The τ_1 value of the ITO/perovskite/passivation layer/spiro is smaller than that of the ITO/perovskite/spiro, which indicates that the interface has fewer defects. The detailed results are shown in Table 2. This conclusion is also consistent with UPS and PL, and shows the ultimately improvement of the electrical performance of PSCs.

In order to better evaluate the trap density of both perovskite films, space-charge-limited current (SCLC) was conduc-

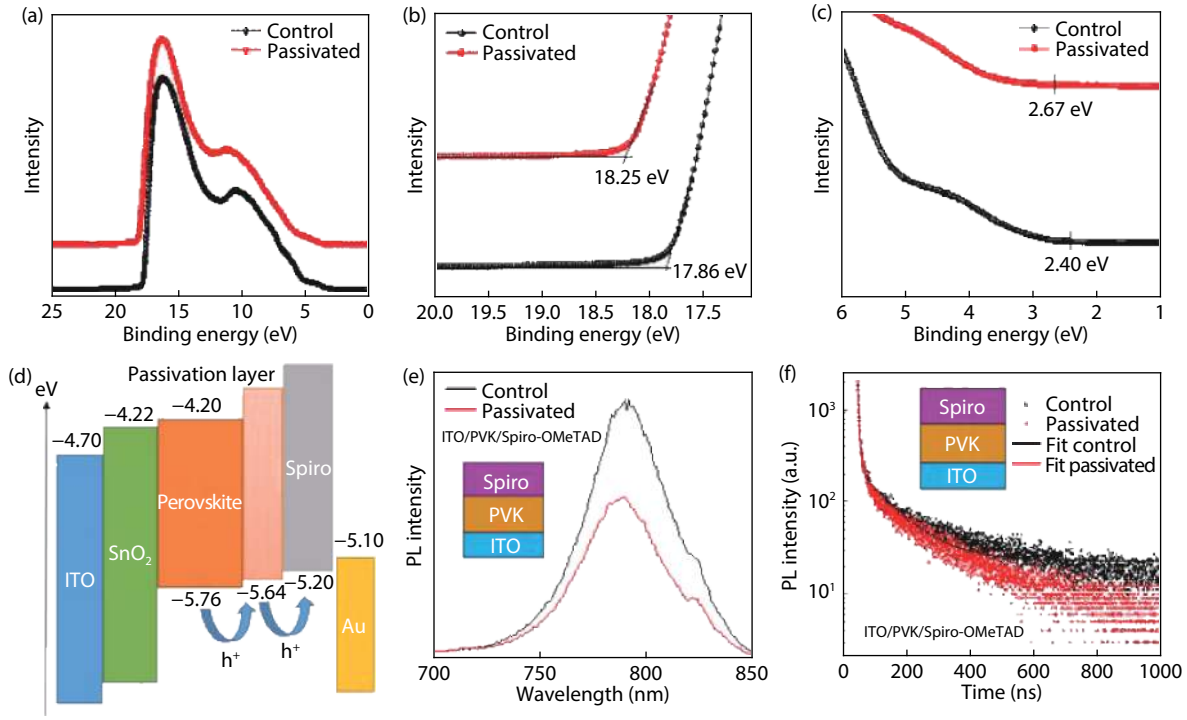

Fig. 4. (Color online) (a) Spectra of ultraviolet photoelectron spectroscopy (UPS). (b) Secondary electron cutoff and (c) valence band region near E_F of the perovskite film without (control) and with MABr (2 mg/mL) deposited on ITO substrate. (d) The energy level diagram of PSCs. (e) Steady-state photoluminescence (PL) and (f) time-resolved PL (TRPL) spectra of the passivated and control perovskite film.

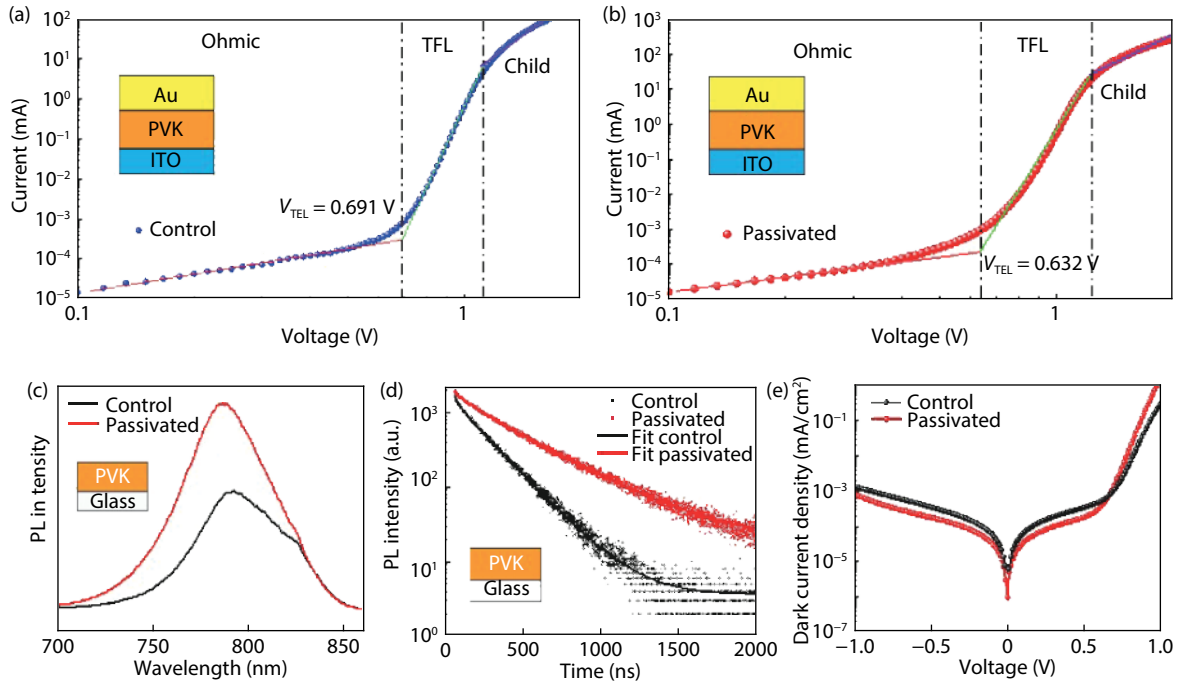

Fig. 5. (Color online) *I*–*V* curves with the device structure of ITO/perovskite/Au, where the perovskite (a) without (control) and (b) with the passivation measured in the dark. (c) Steady-state photoluminescence (PL) and (d) time-resolved PL (TRPL) spectra of the passivated and control perovskite film. (e) The dark *I*–*V* characteristics of the perovskite devices with and without the MABr.

ted under dark conditions with the glass/ITO/perovskite/Au (Figs. 5(a) and 5(b)) device structure. The calculation formula of n_{trap} can be described by[37, 38]:

$$V_{TEL} = en_t d^2/2\varepsilon\varepsilon_0,$$

where V_{TFL} is the trap-filled limit (TFL) voltage, e is the electric charge, d is the thickness of the perovskite layer, ε_0 is the vacuum permittivity, and ε is the dielectric constant of the perovskite layer. The calculated trap state densities are 1.51×10^{16} and 1.38×10^{16} cm^{-3} for the control and passivated perovskite, respectively[39]. It is obvious that the passivated per-

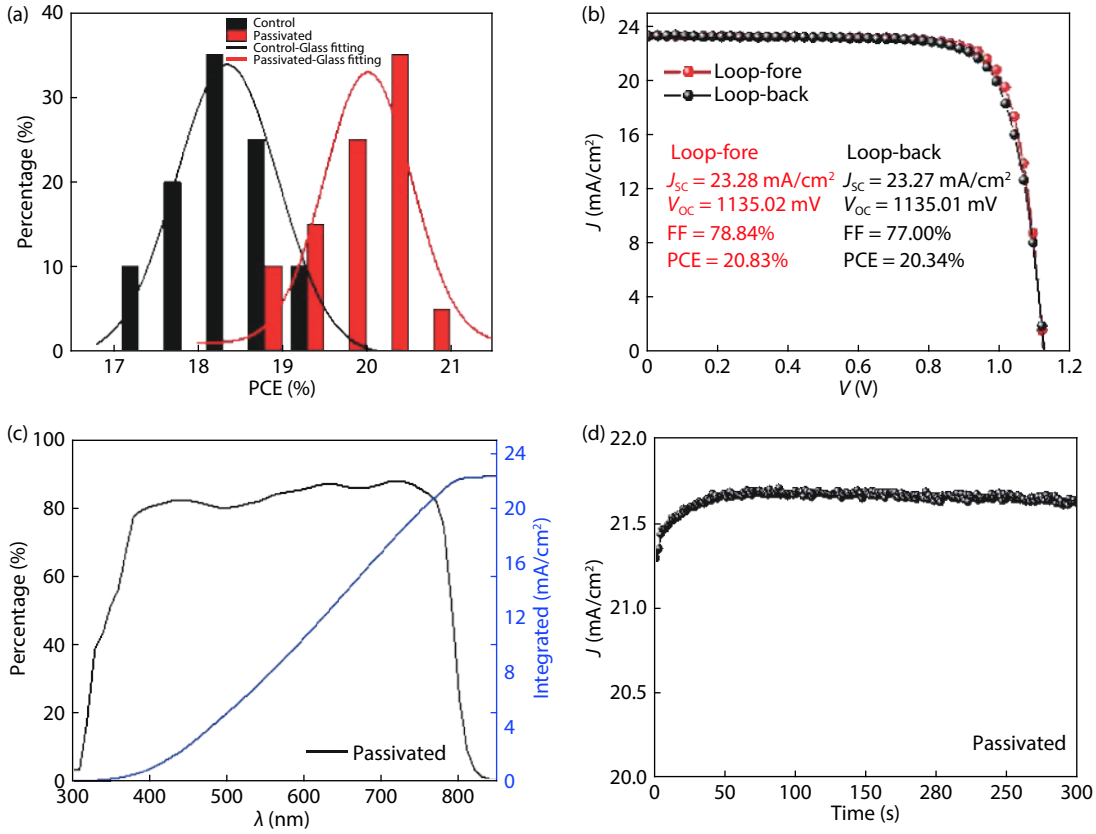

Fig. 6. (Color online) (a) Histogram distribution of the PCE for devices with control (40 cells) and passivated perovskite films (40 cells). (b) *J*–*V* curves and (c) EQE spectra with integrated J_{SC} of the best passivated perovskite devices. (d) Current density measured for 300 s at the steady power output (SPO) with a fixed maximum voltage (0.97 V).

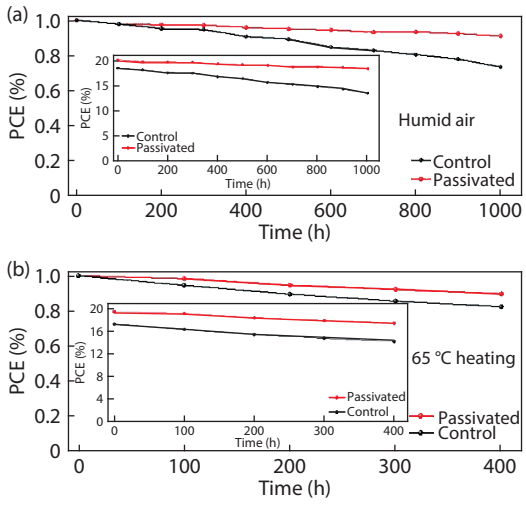

Fig. 7. (Color online) (a) PCEs evolution of devices in ambient air with the room temperature of 25–30 °C, and the humidity of 20%–30%. (b) Devices kept at 65 °C in ambient air with encapsulation for 400 h.

ovskite film has lower n_{trap} value which indicates the reduced surface defects. Figs. 5(c) and 5(d) are the PL intensity and lifetimes of the control and passivated perovskite films with the glass/perovskite structure, respectively. The results show that the PL peak without passivation layer is 780 nm, while the peak of passivated perovskite is 770 nm. The blue shift of emission peak position also confirms the reaction of MABr and PbI_2. In addition, the PL peaks intensity of passivated perovskite film is higher, indicating fewer defects. Therefore, the addition of passivated film significantly suppresses the non-radiative recombination, which is the reason for the improved V_{oc}. This result is also consistent with PL and SCLC. Moreover, in order to evaluate the effect of the modified layer on the photovoltaic performance, a dark *J*–*V* curves were conducted, as shown in Fig. 5(e). The modified layer with better band alignment leads to enhanced electron injection and decreased leakage current density[40].

Eighty samples with or without passivation layer were prepared in different batches, and the average values of PCE are shown in Fig. 6(a), respectively. The average PCE of controlled sample is about 18.40%, while passivated devices is about 20.00%. Fig. 6(b) presents the *J*–*V* curves with forward and reverse scanning directions of champion device with passivated perovskite solar cell. The best-performing device achieves a PCE of 20.83% from forward scan with a V_{oc} of 1.14 V, J_{sc} of 23.28 mA/cm² and FF of 78.83%. Fig. 6(c) shows the EQE curve of PSCs, as we can calculate that the integrated J_{sc} value is 22.34 mA/cm². In addition, the current density is measured at a fixed maximum voltage (0.97 V) and a steady power output (SPO) for 300 s, as shown in Fig. 6(d).

The performance of passivated PSCs was also evaluated from the perspective of device stability, humidity and thermal stability of the device were carried out. Fig. 7(a) is the stability of devices under humidity (20%–30%) without encapsulation. After 1000 hours, the passivated device could maintain 94% of its initial efficiency (from 19.62% to 18.48%). In contrast, the control device only maintains 70% of its initial efficiency (from 18.30% to 12.91%). We also examine the

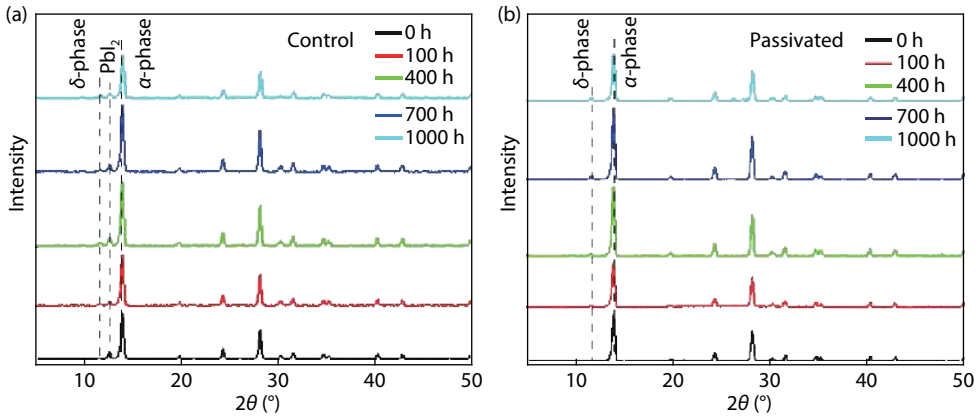

Fig. 8. (Color online) XRD patterns of (a) control and (b) passivated perovskite films after in humid air (with RH: 20%–30%) for 0, 100, 400, 700, and 1000 h.

thermal stability of both devices under ambient air with encapsulation (65 °C), as shown in Fig. 7(b). After 400 hours, the passivated device maintains 90% of its initial efficiency, which means that the passivated devices have better stability under continuous heating at 65 °C.

We also performed XRD test for control and passivated perovskite films in humidity stability test. As we can see in Fig. 8, the yellow phase perovskite peaks appear earlier in the control group, which indirectly reflects that the passivation layer could effectively prevent the water in ambient air from contacting the perovskite absorption layer, thus reduce the influence of water on the perovskite and promote the water stability of the PSCs.

Stability is the most important key characteristic for perovskite solar cells. This research shows that the device stability after passivation has been improved. There are two possible reasons. First of all, excessive PbI_2 is detrimental to device stability[28]. The spin-coated MABr reacts with excessive PbI_2, and then the passivation layer is formed to improve the stability of the device. Furthermore, as previously mentioned, the passivated films with lower trap density are less likely to lead to trap-mediated decomposition. Therefore, the device with passivated layer improves the stability.

4. Conclusion

To promote the electrical properties of PSCs, we introduced a passivation layer between hole transport and perovskite absorber layer. Through the UPS measurement, we found that the energy level after passivation is more matched. The SCLC and TRPL results show that the passivation layer can effectively reduce surface defects and non-radiative recombination, while increase carrier extraction. Ultimately, we obtained a champion device with efficiency of 20.83%. This method also provides enhanced humidity and thermal stability. As a result, the device retains about 94% of its initial PCE after 1000 h under ambient air without encapsulation. We believe that the surface modification strategy will help researchers to achieve efficient and stable PSCs.

Acknowledgements

The authors gratefully acknowledge the supports from National Key Research and Development Program of China (Grant No. 2018YFB1500103), the National Natural Science Foundation of China (Grant No. 61674084), the Overseas Expertise Introduction Project for Discipline Innovation of Higher Education of China (Grant No. B16027), Tianjin Science and Technology Project (Grant No. 18ZXJMTG00220), and the Fundamental Research Funds for the Central Universities, Nankai University (Grant Nos. 63191736, ZB19500204).

References

[1] Yang W S, Noh J H, Jeon N J, et al. High-performance photovoltaic perovskite layers fabricated through intramolecular exchange. Science, 2015, 348(6240), 1234

[2] Dong Q, Fang Y, Shao Y, et al. Electron-hole diffusion lengths > 175 μm in solution-grown $CH_3NH_3PbI_3$ single crystals. Science, 2015, 347(6225), 967

[3] Saidaminov M I, Abdelhady A L, Murali B, et al. High-quality bulk hybrid perovskite single crystals within minutes by inverse temperature crystallization. Nat Commun, 2015, 6(1), 1

[4] Han Q, Bae S H, Sun P, et al. Single crystal formamidinium lead iodide ($FAPbI_3$): insight into the structural, optical, and electrical properties. Adv Mater, 2016, 28(11), 2253

[5] Chu S, Cui Y, Liu N. The path towards sustainable energy. Nat Mater, 2017, 16(1), 16

[6] McMeekin D P, Sadoughi G, Rehman W, et al. A mixed-cation lead mixed-halide perovskite absorber for tandem solar cells. Science, 2016, 351(6269), 151

[7] Kojima A, Teshima K, Shirai Y, et al. Organometal halide perovskites as visible-light sensitizers for photovoltaic cells. J Am Chem Soc, 2009, 131(17), 6050

[8] Kim H S, Lee C R, Im J H, et al. Lead iodide perovskite sensitized all-solid-state submicron thin film mesoscopic solar cell with efficiency exceeding 9%. Sci Rep, 2012, 2, 591

[9] Jiang Q, Zhao Y, Zhang X, et al. Surface passivation of perovskite film for efficient solar cells. Nat Photonics, 2019, 13(7), 460

[10] https://www.nrel.gov/pv/cell-efficiency.html

[11] Hanusch F C, Wiesenmayer E, Mankel E, et al. Efficient planar heterojunction perovskite solar cells based on formamidinium lead bromide. J Phys Chem Lett, 2014, 5(16), 2791

[12] Zhao X, Park N G. Stability issues on perovskite solar cells. In: Photonics. Multidisciplinary Digital Publishing Institute, 2015, 2(4), 1139

[13] Xu T, Chen L, Guo Z, et al. Strategic improvement of the long-term stability of perovskite materials and perovskite solar cells. Phys Chem Chem Phys, 2016, 18(39), 27026

[14] Zheng X, Chen B, Dai J, et al. Defect passivation in hybrid perovskite solar cells using quaternary ammonium halide anions

and cations. Nat Energy, 2014, 2, 17102
[15] Yang W S, Park B W, Jung E H, et al. Iodide management in formamidinium-lead-halide–based perovskite layers for efficient solar cells. Science, 2017, 356(6345), 1376
[16] Wang F, Bai S, Tress W, et al. Defects engineering for high-performance perovskite solar cells. npj Flexible Electron, 2018, 2(1), 1
[17] Meng L, Sun C, Wang R, et al. Tailored phase conversion under conjugated polymer enables thermally stable perovskite solar cells with efficiency exceeding 21%. J Am Chem Soc, 2018, 140(49), 17255
[18] Bai Y, Meng X, Yang S. Interface engineering for highly efficient and stable planar p–i–n perovskite solar cells. Adv Energy Mater, 2018, 8(5), 1701883
[19] Sherkar T S, Momblona C, Gil-Escrig L, et al. Recombination in perovskite solar cells: significance of grain boundaries, interface traps, and defect ions. ACS Energy Lett, 2017, 2(5), 1214
[20] Moriya M, Hirotani D, Ohta T, et al. Architecture of the interface between the perovskite and hole-transport layers in perovskite solar cells. ChemSusChem, 2016, 9(18), 2634
[21] Tan H, Che F, Wei M, et al. Dipolar cations confer defect tolerance in wide-bandgap metal halide perovskites. Nat Commun, 2018, 9(1), 1
[22] Li N, Tao S, Chen Y, et al. Cation and anion immobilization through chemical bonding enhancement with fluorides for stable halide perovskite solar cells. Nat Energy, 2019, 4(5), 408
[23] Wang P, Li R, Chen B, et al. Gradient energy alignment engineering for planar perovskite solar cells with efficiency over 23%. Adv Mater, 2020, 32(6), 1905766
[24] Jiang Q, Chu Z, Wang P, et al. Planar-structure perovskite solar cells with efficiency beyond 21%. Adv Mater, 2017, 29(46), 1703852
[25] Turren-Cruz S H, Hagfeldt A, Saliba M. Methylammonium-free, high-performance, and stable perovskite solar cells on a planar architecture. Science, 2018, 362(6413), 449
[26] Wang Y, Wu T, Barbaud J, et al. Stabilizing heterostructures of soft perovskite semiconductors. Science, 2019, 365(6454), 687
[27] Wang P, Jiang Q, Zhao Y, et al. Synergistic improvement of perovskite film quality for efficient solar cells via multiple chloride salt additives. Sci Bull, 2018, 63(11), 726
[28] Tumen-Ulzii G, Qin C, Klotz D, et al. Detrimental effect of unreacted PbI_2 on the long-term stability of perovskite solar cells. Adv Mater, 2020, 32(16), 1905035
[29] Jeng J Y, Chen K C, Chiang T Y, et al. Nickel oxide electrode interlayer in $CH_3NH_3PbI_3$ perovskite/PCBM planar-heterojunction hybrid solar cells. Adv Mater, 2014, 26(24), 4107
[30] You J, Meng L, Song T B, et al. Improved air stability of perovskite solar cells via solution-processed metal oxide transport layers. Nat Nanotechnol, 2016, 11(1), 75
[31] Xu G, Bi P, Wang S, et al. Integrating ultrathin bulk-heterojunction organic semiconductor intermediary for high-performance low-bandgap perovskite solar cells with low energy loss. Adv Funct Mater, 2018, 28(42), 1804427
[32] Zhang J, Xue R, Xu G, et al. Self-doping fullerene electrolyte-based electron transport layer for all-room-temperature-processed high-performance flexible polymer solar cells. Adv Funct Mater, 2018, 28(13), 1705847
[33] Wang S, Sakurai T, Wen W, et al. Energy level alignment at interfaces in metal halide perovskite solar cells. Adv Mater Interfaces, 2018, 5(22), 1800260
[34] Li X, Bi D, Yi C, et al. A vacuum flash-assisted solution process for high-efficiency large-area perovskite solar cells. Science, 2016, 353(6294), 58
[35] Noel N K, Abate A, Stranks S D, et al. Enhanced photoluminescence and solar cell performance via Lewis base passivation of organic–inorganic lead halide perovskites. ACS Nano, 2014, 8(10), 9815
[36] Du Y, Xin C, Huang W, et al. Polymeric surface modification of Ni-O_x-based inverted planar perovskite solar cells with enhanced performance. ACS Sustain Chem Eng, 2018, 6(12), 16806
[37] Lampert M A. Simplified theory of space-charge-limited currents in an insulator with traps. Phys Rev, 1956, 103(6), 1648
[38] Zhumekenov A A, Saidaminov M I, Haque M A, et al. Formamidinium lead halide perovskite crystals with unprecedented long carrier dynamics and diffusion length. ACS Energy Lett, 2016, 1(1), 32
[39] Zhang M, Chen Q, Xue R, et al. Reconfiguration of interfacial energy band structure for high-performance inverted structure perovskite solar cells. Nat Commun, 2019, 10(1), 1
[40] Wang S, Chen H, Zhang J, et al. Targeted therapy for interfacial engineering toward stable and efficient perovskite solar cells. Adv Mater, 2019, 31(41), 1903691